Carcinogenesis vol.23 no.10 pp.1701–1711, 2002

Interrelationships among angiogenesis, proliferation, and apoptosis in the tumor microenvironment during *N*-methyl-*N*-nitrosourea androgen-induced prostate carcinogenesis in rats

Zhiming Liao[1], Thomas W.-M.Boileau[2], John W.Erdman Jr[3] and Steven K.Clinton[1,4]

[1]Division of Hematology and Oncology, Department of Internal Medicine, The Ohio State University, College of Medicine and Public Health, A434 Starling Loving Hall, 320 West 10th Avenue, Columbus, OH 43210, USA, [2]Department of Human Nutrition, The Ohio State University, Columbus, OH 43210, USA and [3]Division of Nutritional Sciences, University of Illinois, Urbana, IL 61801, USA

[4]To whom correspondence should be addressed
Email: clinton-1@medctr.osu.edu

Proliferation, apoptosis and angiogenesis are critical biologic processes altered during carcinogenesis. Surrogate biomarkers of these processes represent potential intermediate endpoints for short-term intervention studies with preventive and therapeutic agents. We examined the interrelationships among these processes during prostate carcinogenesis induced by *N*-methyl-*N*-nitrosourea (MNU) in male Wistar-Unilever rats. Immunohistochemical and digital image analysis techniques were used to evaluate the proliferation index, the apoptotic index and microvessel density (MVD) in tissue representing stages of prostate carcinogenesis. The proliferation index in the normal glandular epithelium of the prostate is lower than that observed in hyperplastic foci and atypical hyperplasia ($P < 0.01$) and is further increased in carcinoma ($P < 0.01$). Apoptosis in the normal prostate epithelium or hyperplastic lesions is lower than in adenocarcinoma ($P < 0.01$). In parallel to proliferation index, MVD increases as prostate cancer progresses. As tumors enlarge, we observed a predictable change in biomarker expression within the tumor microenvironment. We examined prostate tumors ≥1 cm in diameter and biomarker expression was quantified within the peripheral (outer 1–2 mm), central (perinecrotic) and intermediate (remaining) areas of each tumor. The proliferation index is higher ($P < 0.01$) in the intermediate area than either in the peripheral area or central area. Similarly, the vascular density in the intermediate area is higher ($P < 0.01$) than either in the peripheral or central area. The apoptotic index is higher ($P < 0.05$) in the central perinecrotic core than that in either the intermediate or the peripheral area. In conclusion, we observe that angiogenesis, proliferation and apoptosis are linked biological processes predictably altered temporally and spatially during prostate carcinogenesis in the MNU model. These biomarker changes are similar to those reported in human prostate carcinogenesis and represent potential biomarkers for the assessment of dietary, chemopreventive and therapeutic agents.

Abbreviations: HPF, high power field; H&E, hematoxylin and eosin; MNU, *N*-methyl-*N*-nitrosourea; MVD, microvessel density; PCNA, proliferating cell nuclear antigen; PIN, prostatic intraepithelial neoplasia; TUNEL, terminal deoxynucleotidyltransferase (TdT)-mediated deoxyuridine triphosphate-biotin nick-end labeling.

Introduction

The rapid clinical development of new chemopreventive agents and dietary strategies for prostate cancer prevention is limited by the long periods of time and the great expense required to complete human prostate cancer studies. In addition, the slow progress in validating surrogate biomarkers that can be applied in short-term clinical studies has further inhibited the translation of laboratory and epidemiologic observations to clinical trials. Animal models of prostate carcinogenesis are rapidly being developed (1–7) and provide tools for the pre-clincal assessment of the efficacy and toxicity of novel agents or dietary components. Rodent models also allow for the evaluation of biomarkers that can subsequently be used as surrogate endpoints in the initial short-term human studies that are necessary to define optimal dosing strategies for long-term definitive human prevention studies. The *N*-methyl-*N*-nitrosourea (MNU) androgen-induced model of prostate carcinogenesis in Wistar-Unilever rats has emerged as a valuable tool in this regard (5,7,8). This model has several advantages including the development of a broad spectrum of histopathologic lesions corresponding to progression from hyperplasia to dysplasia and adenocarcinoma. Larger tumors are invasive, capable of metastasizing and emerge from the dorsolateral lobe and anterior prostate, which are embryologically homologous to the site of origin of human prostate cancer (6).

A vast array of biomarkers are currently being evaluated relative to prostate carcinogenesis in order to gain insight into mechanisms whereby novel agents may act, or as predictions of anticancer activity. Those include, but are not limited to, proliferation biomarkers [PCNA (proliferating cell nuclear antigen), ki67 and cyclins], angiogenesis biomarkers [CD31, CD34, Factor VIII-RA, microvessel density (MVD) and vascular endothelial cell growth factor (VEGF)], morphologic biomarkers (nuclear pleomorphism, Gleason grading of tumor architecture), biochemical biomarkers (prostatic-specific antigen), hormonal changes (testosterone, insulin-like growth factor-1) and genetic/regulatory biomarkers (tumor growth factor-β, p53, gene mutations and loss of heterozygosity) (9). Many of these outcomes are intimately related to three of the critical processes common to the carcinogenic cascade in a vast array of tissues: proliferation, apoptosis and angiogenesis (10). Proliferative index, or the proportion of cells actively undergoing cell division, represents the balance between growth promoting and growth suppressing signals derived from cell–cell contact, the extracellular matrix and soluble factors. In general, the carcinogenic process leads to irreversibly activated proliferative signaling pathways that are progressively independent from growth promoting hormones, growth factors and cytokines. In parallel, tumor cells escape from anti-proliferative and pro-differentiation signals (10). Apoptosis represents a necessary pathway in order to maintain a balance between cell renewal and cell attrition within all normal tissue (10). In contrast, prostate and other cancers have established a resistance to apoptosis, which may contribute

significantly to the rate at which tumor volume expands (11,12). The lack of chemopreventive effects on prostate carcinogenesis by certain pro-apoptotic and pro-differentiation agents may be partially a consequence of acquired resistance toward apoptosis (5). Accumulating evidence supports the concept that a developing tumor must establish a pro-angiogenic phenotype in order to grow beyond a few millimeters in size and progress to an invasive and metastatic lesion (10,13). The tumor vasculature provides for the removal of toxic metabolic waste and the delivery of essential nutrients and oxygen for synthetic and metabolic processes critical for cell division and survival (14,15). Thus, angiogenesis may be intimately linked to proliferative and apoptotic rates.

The studies reported herein examine the temporal interrelationships among proliferation, angiogenesis and apoptosis during the progression of prostate carcinogenesis in the MNU androgen-induced model of prostate carcinogenesis in Wistar-Unilever rats (4–6). We further examine the spatial relationships in biomarker expression as influenced by prostate tumor volume. These studies provide additional insight regarding the interpretation of biomarker expression in future studies using this model for the evaluation of novel interventions with therapeutic agents as well as dietary components or chemopreventive agents.

Materials and methods

Animals and diets

The rats employed in this study represent the control diet group (n = 32) from a large study (n = 194) evaluating the ability of dietary lycopene, tomato products and energy restriction to inhibit prostate carcinogenesis (16). Male Wistar-Unilever rats (Harlan, Indianapolis, IN) procured at 5 weeks of age were fed an AIN-93G-based semi-purified diet (Dyets, Bethlehem, NJ) (17) for the duration of the experiment. Rats were housed individually in stainless steel cages, in a room at constant temperature (22°C), with a 12-h dark–light cycle, and were allowed free access to water and unlimited food supplies. Diets were stored at 4°C in the dark with fresh diet provided every 72 h. Rats were weighed weekly, and total food intake was quantified and published elsewhere (16).

Prostate tumor induction

Carcinogen and hormone exposure followed protocols published previously (5,8). At 6 weeks of age, each rat received daily i.p. injections of cyproterone acetate (Sigma Chemical, St Louis, MO) for 21 consecutive days. One day after the last dose of cyproterone acetate (9 weeks of age), rats received daily s.c. injection of 100 mg testosterone proprionate/kg body wt (Sigma Chemical) in 0.5 ml soybean oil for 3 days. One day after the last testosterone proprionate injection all rats received a single i.v. dose (50 mg/kg body wt) of MNU (Ashe Stevens, Detroit, MI) via the tail vein under metophane anesthesia. MNU was initially wetted with 3% acetic acid and stored at –20°C. Immediately prior to injection, MNU was dissolved in saline at 10 mg/ml with a final pH of 5.5. One week after MNU administration, rats received continuous exposure to testosterone via two subcutaneous implants (1.02 mm ID×2.16 mm OD×2.54 cm length silastic laboratory tubing; Dow Corning, Midland, MI) each containing 30 mg crystalline testosterone (Sigma Chemical). Testosterone was drawn into the implants under vacuum pressure and the ends were sealed with silicone adhesive (Dow Corning). Implants were inserted subcutaneously in the dorsolumbar region using sterile techniques and the wounds sealed with surgical glue. All animal procedures were approved by the University of Illinois Laboratory Animal Care Advisory Committee.

Necropsy

Rats were monitored daily throughout the experiment. Those surviving until the planned necropsy at 64 weeks or those earlier exhibiting signs or symptoms of progressive prostate cancer such as reduced urine output, decreased food intake or weight loss, were killed by CO_2 inhalation. Immediately thereafter, the bladder, prostate (dorsolateral, ventral and anterior also known as the coagulating gland) and seminal vesicles were removed *en bloc* and placed in 10% neutral-buffered formalin.

Histopathology

The fixed tissue was dissected into seven components for microscopic evaluation: (i) bladder, (ii) right ventral lobe, (iii) left ventral lobe, (iv) right dorsolateral lobe, (v) left dorsolateral lobe, (vi) right seminal vesicle and (vii) left seminal vesicle. Dorsolateral and ventral lobes were each further dissected sequentially. Each seminal vesicle (right and left) was dissected into four to five sequential sections. All samples were embedded in paraffin using a Tissue Embedding System (Shandon Histocentre 2, Shandon, Pittsburgh, PA). Paraffin-embedded tissue blocks were sectioned at 3.5 μ and transferred to Superfrost plus slides (Fisher Scientific, Pittsburgh, PA). After heating at 60°C in an oven for 30 min the slides were stained with hematoxylin and eosin (H&E) by an automated robotic slide stainer (Leica Autostainer XL, Leica Instrument, Nussloch, Germany). Mounting medium (Cytoseal 60, Richard-Allan Scientific, Kalamazoo, MI) was applied and sections covered with glass cover slips. Slides were blindly evaluated by two investigators (S.K.C. and Z.L.) for histopathologic classification according to criteria published previously (4,5). Virtually all rats examined exhibited some focal hyperplasia of the prostatic epithelium defined as an accumulation of cells without invasion or pleomorphism. Carcinoma *in situ* was characterized as an epithelial proliferative lesion with cellular characteristics of carcinoma (such as increased ratio of nuclear/cytoplasm, nuclear and cellular pleomorphism, nuclear hyperchromasia and loss of cell polarity), but no evidence of invasion through the basement membrane. Adenocarcinoma was characterized as a proliferative lesion with clear evidence of invasion into the stroma and/or other tissues, and is further subclassified based on the degree of differentiation. A well-differentiated adenocarcinoma exhibit fairly homogeneous small glands or acini, while the tumor cells have fairly homogeneous cellular features that are similar to normal epithelium and show little nuclear pleomorphism. Moderately differentiated carcinomas consist of glands with more heterogeneous sizes and shapes lined by cells with moderate nuclear pleomorphism. Poorly differentiated adenocarcinomas contain poorly formed glands or sheets of tumor cells with marked cellular and nuclear pleomorphism. Necrosis is typically present in the center of poorly differentiated carcinomas and occasionally seen in moderately differentiated tumors.

Proliferation index

The proliferation index is calculated as the percentage of nuclei-stained positive with anti-PCNA antibody. PCNA is a co-factor for DNA-polymerase δ expressed in both the S phase of the cell cycle and during DNA synthesis associated with DNA repair (18). Quantification of PCNA mRNA in many cells and malignant cell lines is typically correlated with the entry into the cell cycle, S phase and the late stage of mitosis (18). However, PCNA protein is primarily localized in the nucleus of cells that are in the S phase (18). Paraffin-embedded tissue sections were prepared and processed by deparaffinization, rehydration and washing. The slides were heated in citrate buffer (10 mM, pH 6.0) at 100°C for 3 min, and cooled to room temperature to unmask the PCNA. The subsequent steps were completed in an OptiMax Automated Cell Staining System (BioGenex, San Ramon, CA). All slides were washed with PBS three times between steps. Endogenous peroxidase was quenched with 3% H_2O_2 in methanol for 10 min. Non-specific binding was minimized with blocking for 20 min with horse serum (BioGenex). Rabbit anti-PCNA antibody (Dako, Carpinteria, CA) was incubated for 30 min, followed by a 20 min incubation with a universal biotinylated horse anti-rabbit antibody (BioGenex). After three washings, a strepavidin horse radish peroxidase was added and incubated for 20 min. Sections were stained with diaminobenzidine chromogen solution (Dab) for 15 min, counterstained with hematoxylin for 1 min, and mounted. The same procedures with control horse serum or omission of primary antibodies were included as negative controls.

The images from PCNA-stained sections were captured at 400-fold magnification by a digital camera (Spot RT, Diagnostic Instruments, Sterling Heights, MI) using bright field microscopy (Nikon ECLIPSE E 800, Tokyo, Japan). The images were transmitted to a computer (6500 Pentium III WorkStation, Dell Computer, Round Rock, TX), saved and analyzed by image analysis software (Image-Pro Plus 4.1, Media Cybernetics, Silver Spring, MD). There are five basic steps for image analysis of PCNA-labeled sections: image input, image calibration, image segmentation, object counting and data analysis. In brief, positive (Dab brown staining) and negative (hematoxylin blue staining) nuclei are segmented into two classes of objects, red channel for positive nuclei and green for negative-stained nuclei using multiple filters followed by quantification of positive-stained and negative-stained objects. The data are then used to calculate the proliferation index based on the following formula: index (%) = $L\times100 / (L + C)$, where L indicates labeled cells and C indicates counterstained, unlabeled cells.

In situ apoptotic cell detection

The ApopTag *in situ* detection kit (Oncor, Gaithersburg, MD) was employed following the manufacturer's recommendations (19). This procedure is often referred to terminal deoxynucleotidyltransferase (TdT)-mediated deoxyuridine triphosphate-biotin nick-end labeling, or TUNEL assay. In brief, sections undergo deparaffinization, rehydration and washing, followed by treatment

with 20 μg/ml of proteinase K for 15 min at room temperature and repeat washing. Endogenous peroxidase activity was quenched with 3% H_2O_2 in PBS for 5 min. The 3′-hydroxy DNA strand breaks were enzymatically labeled with digoxygenin nucleotide via TdT and incubated for 1 h at 37°C, and the reaction terminated with a stop buffer. Sections were then incubated with anti-digoxygenin peroxidase for 30 min at room temperature, washed, stained with 3-3′ diaminobenzidine substrate, counterstained with methyl green and mounted. Positive and negative control slides provided with the kit are used in each assay to insure consistency. Substitution of TdT with distilled water also serves as a negative control. Three representative areas lacking necrosis were selected on each slide and both apoptotic nuclei and total tumor cell nuclei are counted at a 400-fold magnification using methods as described above for the proliferation index. The apoptotic index (AI) is expressed as percentage, AI (%) = $A\times100$ / (A + C), where A indicates apoptotic cells and C indicates counterstained, unlabeled cell.

CD31 immunohistochemical staining

Platelet endothelial cell adhesion molecule-1 (PECAM-1 or CD 31) is highly expressed on the surface of endothelial cells and serves as an ideal target for immunohistochemical staining. Sections undergo deparaffinization, rehydration and washing, followed by heating for 20 min at 100°C in 100 mM citrate buffer (pH 6.0) to accomplish antigen retrieval. The subsequent steps are completed in an OptiMax Automated Cell Staining System (BioGenex) as described above for PCNA except for a change to mouse anti-rat CD31 as the primary antibody (Pharmingen, San Diego, CA). Mouse isotype antibodies were used as negative controls. The same procedure without primary antibody was also included as a negative control.

The images from CD31-stained sections were captured (200×), transmitted, saved and subsequently analyzed by the image analysis software (Image-Pro Plus 4.1) as described above. Multiple tools and filters were used to precisely segment brown (Dab) staining blood vessels from the background. Each image was then reviewed to insure that adjacent or branching vessels were appropriately defined. The number of blood vessels per high power field, vessel diameter, percent area of blood vessels per high power field (200×) and roundness of blood vessels were calculated using image analysis software (Image-Pro Plus 4.1, Media Cybernetics). MVD was defined as the total number of microvessels per 200× field (1.0×1.5 mm^2 area) at three representative sites of each section. Necrotic areas of carcinomas were not included in the analysis.

Analysis and statistics

Quantitative data derived from analysis of digitized images were initially evaluated by one way analysis-of-variance (ANOVA). Fisher's protected least-significant difference was subsequently employed for pairwise comparisons only if the ANOVA was initially significant at $P < 0.05$. StatView 5.01 software (SAS Institute, Cary, NC) was employed.

Results

Histology

Overall, prostate cancer incidence is 63% in the subgroup of rats fed the AIN-93G-based diet. In all the sections of rat prostate we examined in this subgroup, 56% shows evidence of hyperplasia, 18% with atypical hyperplasia, 18% with well-differentiated adenocarcinoma, 23% with moderately differentiated adenocarcinoma and 52% with poorly differentiated adenocarcinoma. The location of tumors in this model is almost exclusively the dorsolateral lobe and anterior prostate gland. Multiple foci of carcinoma are often identified in the same rat with tumors of various sizes, differentiation and grade observed. Hyperplasia of the seminal vesicle is very common (>80% of rats). Some large prostate tumors disrupt the normal architecture of the prostate gland and invade adjacent lobes and the precise origin of the carcinoma may be difficult to identify. Rats with larger poorly differentiated tumors occasionally have peritoneal carcinomatosis or metastases in the liver, bladder, lung or kidney.

Proliferation

The epithelium of the prostate gland exhibits a low and homogeneous proliferation rate. We observed only one to three PCNA-positive nuclear-stained cells per high power field in the dorsolateral lobe, ventral lobe or seminal vesicle (Figure 1). The proliferation index increases significantly during the progression of prostate carcinogenesis from hyperplasia to adenocarcinoma (Figure 1). The mean proliferation index (Table I) in normal prostate epithelial nuclei is 1.9 ± 1.4% (mean ± SD), whereas those in prostate lesions are 18.4 ± 6.6% in hyperplasia, 27.1 ± 9.8% in atypical hyperplasia, 37.3 ± 16.7% in well-differentiated adenocarcinoma, 63.7 ± 11.1% in moderately differentiated adenocarcinoma and 79.4 ± 19.2% in poorly differentiated adenocarcinoma. In addition, we observe ~2–4 mitosis/high power field (HPF) in H&E sections of larger and more poorly differentiated adenocarcinomas while mitoses are not observed in well-differentiated cancers, pre-malignant lesions or the normal epithelium.

Within the larger prostate cancers, we observed that the proliferation rate varies in different locations with the tumor (Figure 2). Proliferation (53 ± 20%, Table II) in the intermediate area is higher ($P < 0.05$) than the peripheral area (18 ± 9%) and the central necrotic area (20 ± 13%). The proliferation index is not significantly different between the outer peripheral area and the peri-necrotic central area.

Apoptosis

Very little apoptosis (0.1 ± 0.1%) is noted in the prostate epithelium (Table I). The apoptotic rate increases significantly in adenocarcinomas (1.0 ± 0.6% in well-differentiated adenocarcinoma, 1.2 ± 0.6% in moderately differentiated adenocarcinoma and 2.6 ± 1.4% in poorly differentiated adenocarcinoma) compared with normal epithelium and that showing hyperplasia (0.5 ± 0.6%) or atypical hyperplasia (0.4 ± 0.4%) ($P < 0.01$). The apoptotic index is not significantly different among normal epithelium, hyperplasia and atypical hyperplasia. Dramatic intra-tumor variation in the apoptotic index is also noted in the larger adenocarcinomas (Figure 3). Apoptotic index in the peri-necrotic central area is ~15-fold higher (7.5 ± 3.1%) than in the outer peripheral area (0.5 ± 0.6%) and more than double ($P < 0.05$) that quantified in the intermediate area (3.0 ± 1.92%, Table II, Figure 3).

Vascularity

Microvessels in the rat accessory sex glands are evenly distributed in the stroma around each glandular element (Figure 1). The MVD (average number of microvessels per high power field, 200×) is fairly constant in all lobes of the non-malignant rat prostate gland (dorsolateral lobe, ventral lobe, seminal vesicle and coagulation gland). MVD shows a significant increase as the pathologic grade of prostate cancer becomes more undifferentiated during the carcinogenic process (Table III and Figure 1). MVD is highest in poorly differentiated adenocarcinoma (45.0 ± 20.3/HPF) followed by moderately differentiated adenocarcinoma (23.6 ± 9.9/HPF), well-differentiated adenocarcinoma (15.4 ± 4.4/HPF), atypical hyperplasia (15.0 ± 6.8/HPF) and hyperplasia (11.8 ± 5.5/HPF), respectively (Table III). In addition, we also evaluated total vascular area within tissue sections and observed a strong correlation with vascular density. Overall, the mean diameter of vessels changed little during carcinogenesis (Table III). As is true for apoptosis and proliferation, we observed intra-tumor variation in vascular density (Table II and Fig. 4). The outer peripheral area and the central peri-necrotic area have similar vascularity scores with 20 ± 9 and 18 ± 12 microvessels/HPF in contrast to the intermediate area exhibiting 44 ± 16/HPF ($P < 0.01$ *vs* other areas, Table II). The vessels in adenocarcinoma typically exhibit chaotic, sinusoid and dilated

patterns (Figure 1) in contrast to the more regular patterns observed in lower grade lesions and normal tissue.

Discussion

Rodent models of prostate carcinogenesis that mimic human disease provide opportunities to rapidly evaluate novel preventive or therapeutic interventions, characterize biomarkers and assess efficacy and safety issues. Our studies in the MNU androgen-induced rat model of prostate carcinogenesis demonstrate strong similarities to human prostate cancer in histopathologic progression and biomarker expression. Several findings suggest that the MNU model is relevant to human

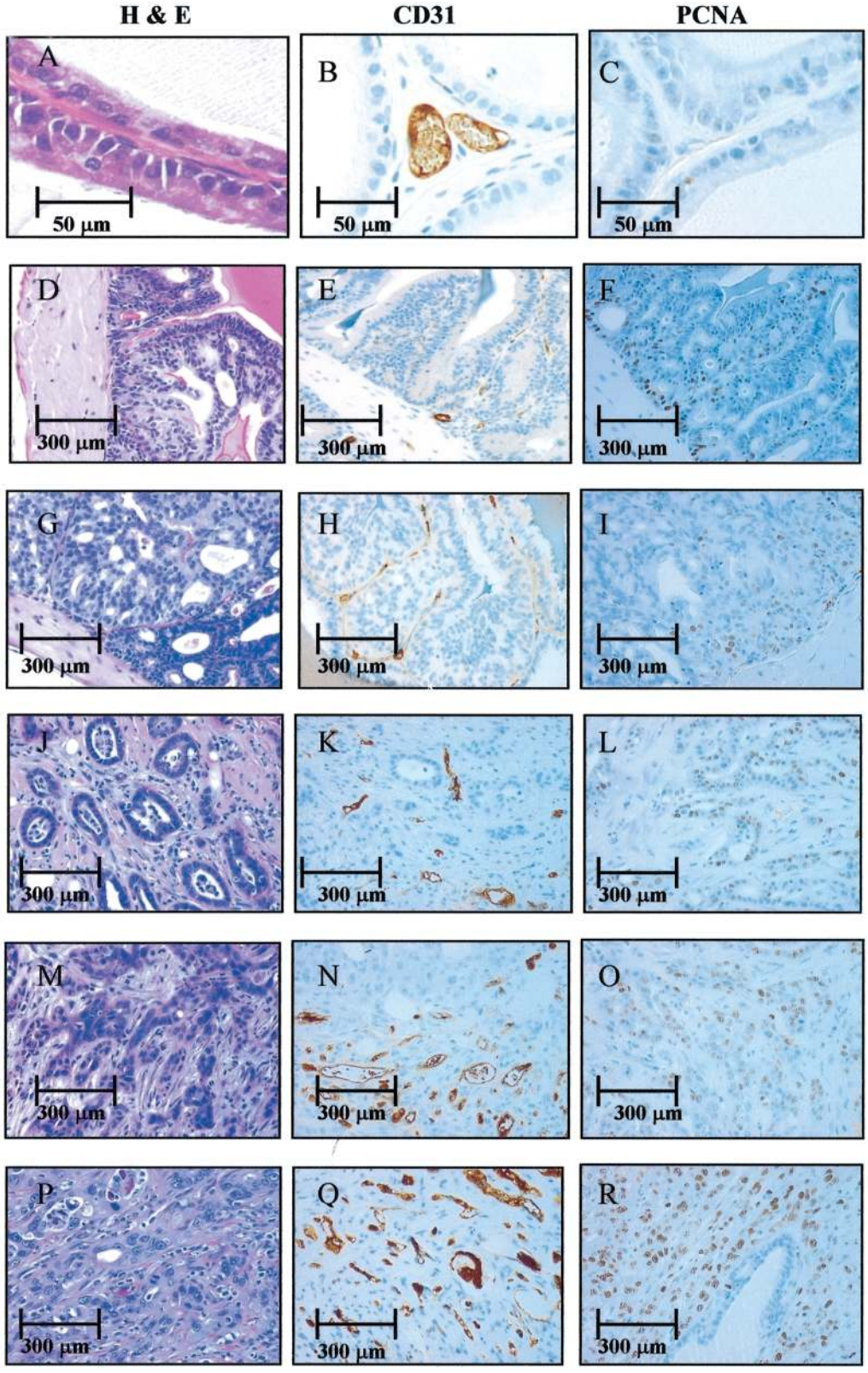

Table I. Proliferation index and apoptotic index in MNU-induced rodent prostate cancer

	Proliferation index (%)	Apoptotic index (%)
NSPC sites*	1.9 ± 1.4^{a} ($n = 15$)	0.1 ± 0.1^{a} ($n = 5$)
Hyperplasia	18.4 ± 6.6^{b} ($n = 14$)	0.5 ± 0.6^{a} ($n = 5$)
Atypical hyperplasia	27.1 ± 9.8^{c} ($n = 9$)	0.4 ± 0.4^{a} ($n = 5$)
Well-differentiated adenocarcinoma	37.3 ± 16.7^{d} ($n = 6$)	1.0 ± 0.6^{b} ($n = 5$)
Moderately-differentiated adenocarcinoma	63.7 ± 11.1^{e} ($n = 4$)	1.2 ± 0.6^{b} ($n = 5$)
Poorly-differentiated adenocarcinoma	79.4 ± 19.2^{f} ($n = 15$)	2.6 ± 1.4^{c} ($n = 5$)

The data represent the mean ± SD. Mean with different superscript indicates $P < 0.01$ by one-way ANOVA and Fisher's protected least significant difference. *NSPC, no significantly pathological change.

disease: (i) the proliferation index increases as prostate cancer progresses; (ii) the apoptotic index increases significantly in prostate cancer, but not in hyperplasia and atypical hyperplasia when compared with normal epithelium; (iii) MVD increases progressively during prostate carcinogenesis; (iv) predictable spatial variations in biomarker expression occur within prostate tumors as they expand in volume; and (v) digital image analysis can be employed easily for the quantitative and objective assessment of biomarkers in histopathologic specimens. Each of these findings in the MNU model are discussed relative to human prostate carcinogenesis.

Constitutive activation of growth signaling pathways, a failure to respond to growth inhibitors and a lack of terminal differentiation are all central concepts of cancer progression that contribute to the greater proliferative rate observed in tumors compared with normal cells of a specific tissue. PCNA has emerged as an easily reproducible immunohistochemistry biomarker of proliferation in fixed tissues. PCNA is a non-histone nuclear protein whose expression increased in G_1, reaches its highest level in S phase, declines during the G_2 phase, and is not detectable in late G_2 and G_0 phases (20). We observe that the progression of prostate carcinogenesis in the MNU model is associated with a profound increase in PCNA labeling ranging from ~2% in normal epithelial cells to 18–28% in hyperplastic lesions, to 37–64% in adenocarcinomas of varying differentiation. Several other investigators have employed PCNA labeling in the rodent prostate and support our observations of increased PCNA labeling with prostate tumor progression. Testosterone and estradiol administration in rats induced low-grade prostatic intraepithelial neoplasia (PIN) with a proliferative rate of 10.4 ± 2.2% and high-grade PIN with a proliferative rate of 27.3 ± 8.4 in contrast to the labeling index of 0% in the normal epithelium by PCNA immunostaining (1). A recent rat study using cadmium exposure reports proliferative rates of 35 ± 15% in dysplastic lesions compared with 12 ± 9% in the normal and hyperplasia (3). In the well-differentiated androgen-dependent Dunning prostate adenocarcinoma (R3327H) the proliferative index is 50 ± 6% and reduced by approximately half with castration (21). In general, proliferative rates in rodent models of carcinogenesis are greater than those in human malignancies although a progressive increase in the labeling index appears to be parallel to that observed in the MNU model. The proliferation index, based upon PCNA labeling, in a comprehensive series of human prostate cancer samples shows 1.62 ± 0.17% (mean ± SD) in normal prostate epithelium, 7.45 ± 0.94% in low-grade PIN, 10.90 ± 1.0% in high-grade PIN and 17.60 ± 2.30% in prostatic adenocarcinoma (22,23). Prostate malignancies with a higher Gleason score, indicating poor differentiation, or more advanced stage typically show a higher proliferation index. PCNA labeling of 23% in prostate cancer with a total Gleason score of 6 or below and 46% in those with Gleason score of 7 or above was observed (24), with higher rates in metastatic sites (27.7 ± 19.1%) compared with primary lesions in the prostate (14.1 ± 9.8%) (2). Other surrogate markers of proliferation are also being evaluated in human and rodent studies with similar trends observed. Ki-67 (MIB-1) is expressed in all phase of the cell cycle except in G_0. Anti-Ki67 (MIB-1) antibody reacts with a nuclear protein expressed in the G_1, G_2, S and M phases of the cell cycle and has good staining in frozen section and smear, but not in paraffin tissue (25). Changes in the proliferation index during prostate carcinogenesis with Ki-67 staining are parallel to that observed with PCNA staining (24,26–29). Other investigators have tried to quantify the mitotic index based upon the number of observed mitotic figures. In general, the mitotic index increases with prostate cancer progression, although the absolute rates of visualized mitotic figures are typically low

Fig. 1. Histopathology and immunohistochemistry of prostate tissues from Wistar-Unilever rats treated with MNU and androgens. All images were captured at 400× magnification. The left column contains the H&E-stained sections (**A**, **D**, **G**, **J**, **M**, **P**), the middle column represents CD31 staining (**B**, **E**, **H**, **K**, **N**, **Q**) and the right column (**C**, **F**, **I**, **L**, **O**, **R**) shows PCNA labeling. The dorsolateral lobe of the prostate exhibits no significant pathologic changes (A–C). The normal epithelium consists of single layer of cuboidal cells admixed with basal cells, mature and well-formed blood vessels (B) and a rare PCNA-labeled nucleus (C). Hyperplasia of the seminal vesicle shows increased cell number and cell layer, hypertrophic cells (increase cell size) and hyperchromatic nuclei, but no significant pleomorphism and invasion of the basement membrane (D–F). Blood vessels are close to the base of the epithelium, which shows greater PCNA labeling than cells near the lumen (E). In contrast, atypical hyperplasia with cells showing a loss of cellular polarity, moderate nuclear pleomorphism and a cribriform glandular pattern (G–I) with increases, but fairly homogeneous blood vessels surrounding the epithelium (H) as compared with (E). Similar to hyperplasia, PCNA labeling is more frequent in the basal layer (I). Well-differentiated adenocarcinoma consists of fairly uniform small glands lacking basal cells, which is more readily seen in higher power fields (B). Stromal invasion is often seen (J–L). Blood vessels are more irregular with variable size and shape (K) compared with pre-malignant lesions. PCNA staining is increased and distributed throughout the tumor (L) as compared with non-malignant sites (C, F, I). A moderately differentiated adenocarcinoma shows poorly formed glands varying in size and shape with extensive stromal invasion (M–O), increased nuclear to cytoplasm ratio (M), abundant sinusoidal and dilated blood vessels (N), and more intense and numerous PCNA staining (O). A poorly differentiated adenocarcinoma (G–I) exhibits a characteristic sheet of malignant cells with marked nuclear and cellular pleomorphism, sinusoid and dilated blood vessels (H), and more intensive PCNA staining (R) than in less aggressive lesions.

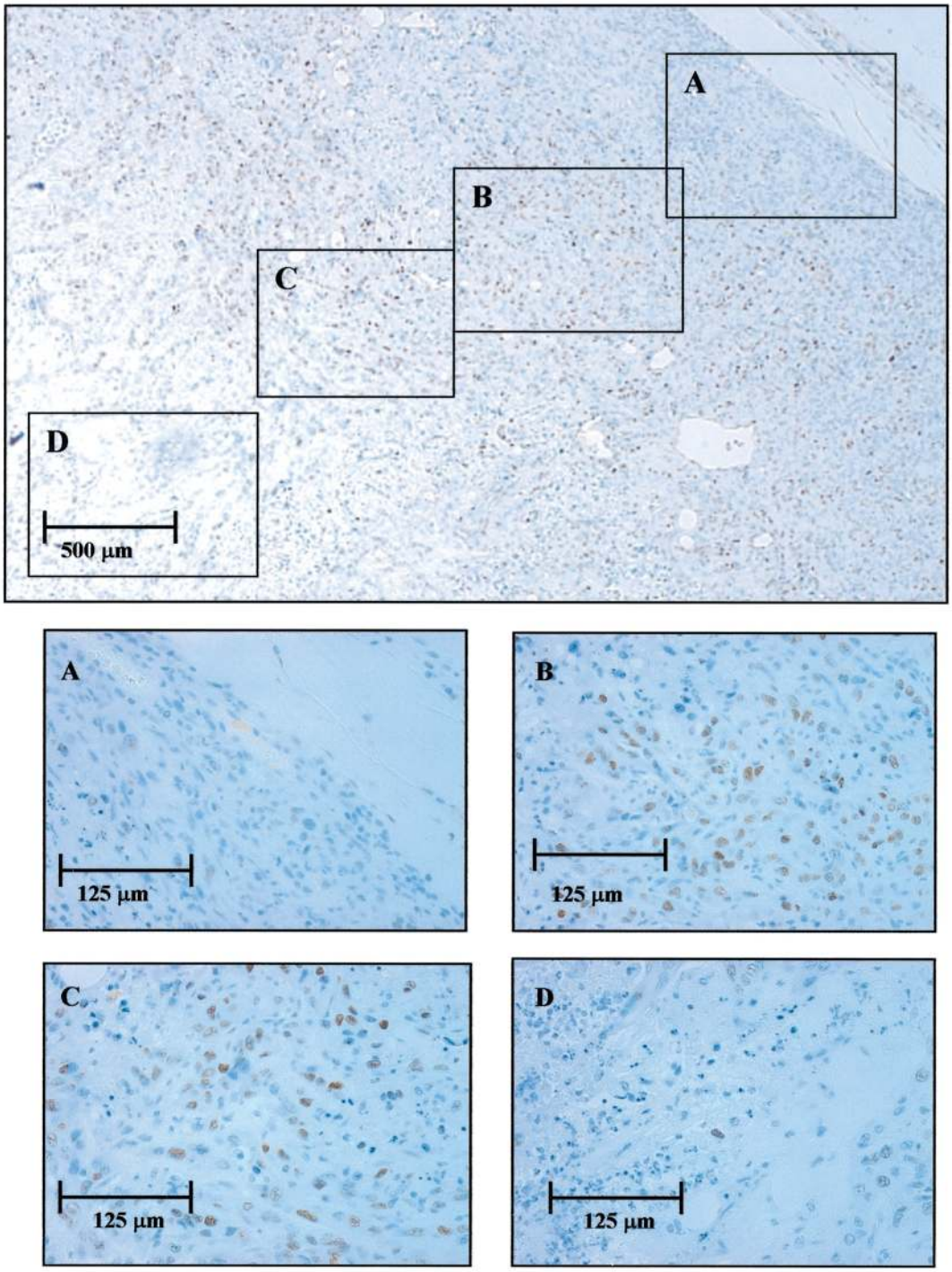

Fig. 2. Representative images of a large (1 cm) poorly differentiated prostate adenocarcinoma with PCNA labeling. (Top) A low power field (40×) illustrates the gradient in PCNA labeling from the surface of the tumor (upper right corner) to the central core (lower left corner). A high power field (400×) shows the outer 500 μm of the tumor (**A**). We typically observe an outer band measuring 100–500 μm characterized by less active cell proliferation. The most active proliferation within the larger prostate tumors extends from ~100–1000 μm from the surface to the central necrotic core (**B** and **C**). The central necrotic core of large tumors and occasional patchy necrotic areas expending further towards the surface show very little PCNA staining (**D**). Necrosis is characterized by loss of nuclear and cell morphology, fragmentation or disappearance of nuclear and cellular membranes admixed with inflammatory cells.

(30,31). Mitosis in benign human prostate lesions is rarely seen, with an index of only 0.001 ± 0.001% (mean ± SE) in benign prostatic hyperplasia, 0.053 ± 0.024% in low-grade PIN, 0.095 ± 0.043 % in high-grade PIN and 0.110 ± 0.044% in cribriform adenocarcinoma (31). We conclude that PCNA is a readily quantifiable and reproducible marker of proliferation in the MNU model and the index increases with tumor progression, and thus mimics human prostate carcinogenesis.

A number of investigators have suggested that the development of new interventions for prostate cancer prevention and treatment should focus upon enhancing apoptosis (11). Clearly, evidence is accumulating that tumor cells demonstrate an

Table II. Comparison of PCNA, apoptosis and CD31 staining in various areas of poorly differentiated adenocarcinoma in rat prostate (mean ± SD)*

Area vessels/HPF)	Proliferation index (n = 10, %)	Apoptotic index (n = 7, %)	CD31 count (n = 9, vessels/HPF)
Peripheral	18.7 ± 9.6[a]	0.5 ± 0.6[a]	20.4 ± 9.0[a]
Intermediate	53.8 ± 20.3[b]	3.0 ± 1.9[b]	44.9 ± 15.8[b]
Peri-necrotic	20.5 ± 13.5[a]	7.5 ± 3.2[c]	18.1 ± 12.3[a]

*Mean with different superscript indicates $P < 0.05$ by one-way ANOVA and Fisher's protected least significant difference.

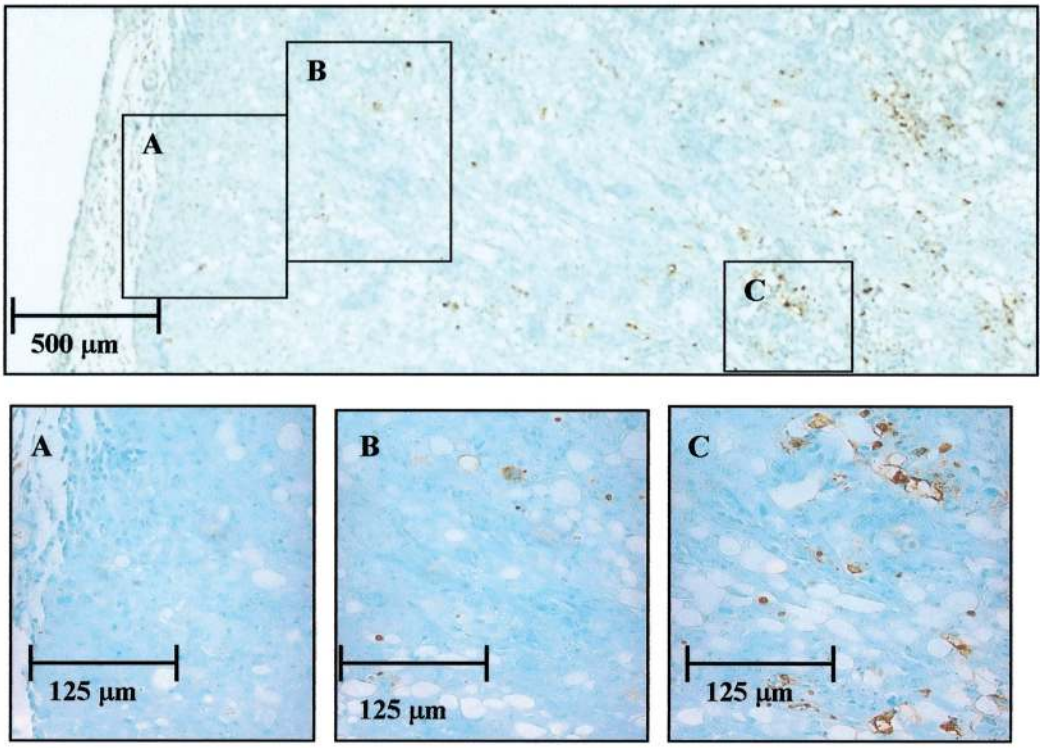

Fig. 3. A representative image of a large (1 cm) poorly differentiated prostate adenocarcinoma stained by ApoTag methods. (Top) A low power field (40×) illustrates the gradient in ApoTag labeling from the surface of the tumor (left) to the central core (right). The rare apoptotic cells in the peripheral area (outer 100–500 μm) of the tumor were observed (**A**). The intermediate area extending from the outer 500 μm to the central necrotic core shows a greater density in the number of apoptotic cells (**B**). The necrotic core and areas immediately adjacent show extensive ApoTag staining involving single cells as well as groups of cells (**C**).

enhanced ability to survive harsh environments and deprivation of survival signals compared with normal cells (10). We observed very low apoptotic rates (0.05 ± 0.13%) in the normal epithelium in the rat model that is in parallel to the low proliferative index. In normal human prostate tissue, the apoptotic rate is also low but varies slightly based upon the location within prostate glands. The index based upon ApoTag methods is 3.3% in peripheral zone, 1.4% in the central zone and 1.8% in the transition zones (32). In comparison, the apoptotic index of only 0.018 ± 0.033% in normal human prostate stroma, and 0.076 ± 0.087% in normal prostate epithelium was reported using *in situ* end labeling (29). As MNU-induced prostate cancer advances in grade and tumor size we see a significant and progressive increase in the proportion of cells undergoing apoptosis, an observation supported by several other studies in humans (33–35). For example, in human prostate specimens the apoptotic index is 0.264 ± 0.033 (mean ± SEM) in normal prostate, 0.679 ± 0.146% in low-grade PIN, 0.749 ± 0.108% in high-grade PIN, 1.282 ± 0.137% in moderately differentiated adenocarcinoma and 2.098 ± 0.186% in poorly differentiated adenocarcinoma (33). A higher apoptotic index is positively correlated with higher Gleason grade and with more advanced human prostate cancer (36) as we observed in the MNU model. Others have also reported increased apoptosis during the early stages of testosterone propionate and 17β-estradiol benzoate-induced prostate cancer initiation in male Noble rats with apoptotic index of 1.19 ± 0.55% in normal epithelia, 0.93 ± 0.26% in low-grade PIN and 3.23 ± 1.25% in high-grade PIN (1). Multiple approaches have been used for the treatment of prostate cancer. The concept that effective prostate cancer prevention or therapy is associated with increased apoptosis is supported by several studies. For example, androgen deprivation by either castration or a 5α-reductase inhibitor-like finasteride can cause apoptosis in the human prostate cancer (37) and in rodent models (38–40). Furthermore,

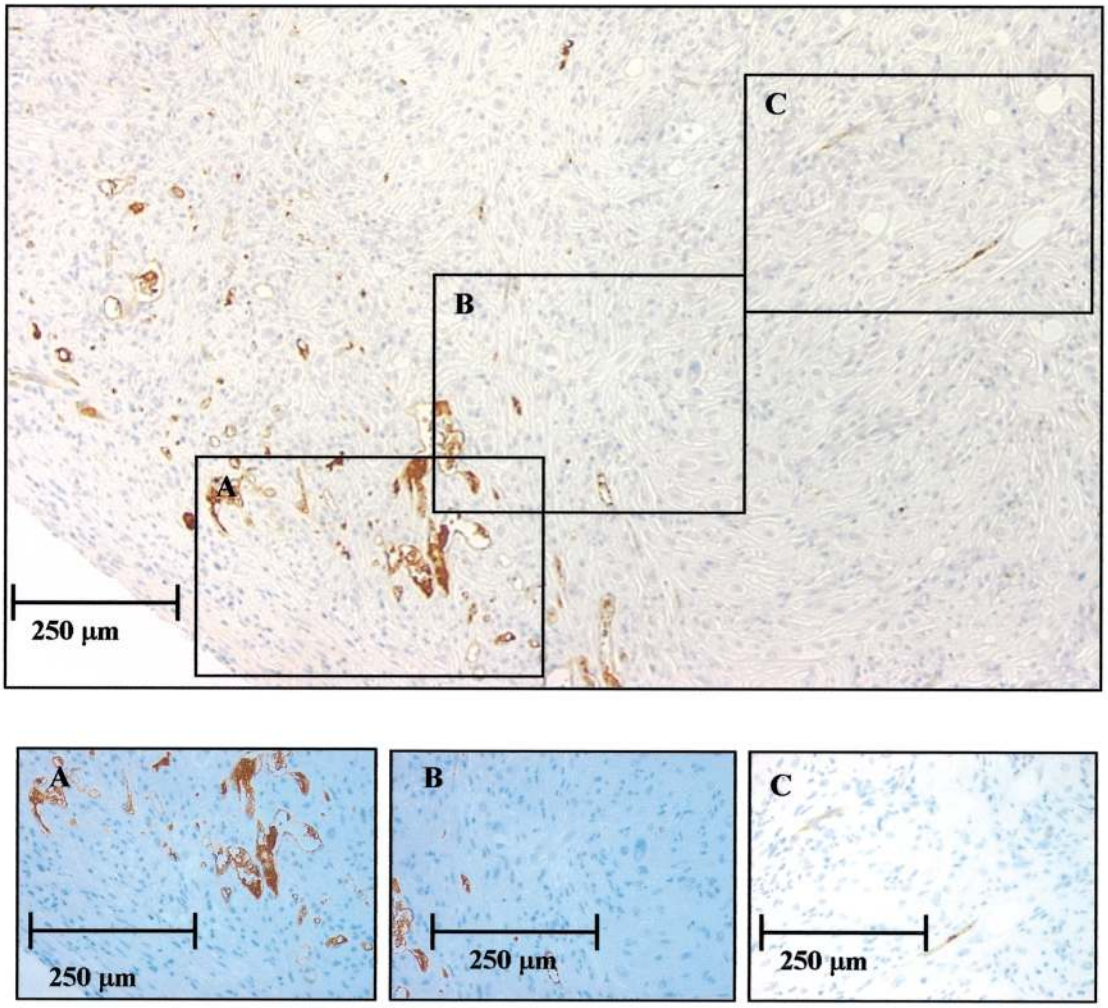

Fig. 4. A representative image of a large (1 cm) poorly differentiated rat prostate cancer stained for the endothelial marker CD31. (Top) A low power field (40×) illustrates the typical gradient in vascular density that we observe in large tumors from the peripheral area (lower left) to the central necrotic area (upper right). We typically observe a thin peripheral layer of tumor cells ~100–150 μm thick where little vascular staining is observed (**A**). There is a dramatic increase in staining that typically extends for ~250 μm immediately adjacent to the relatively poorly vascularized peripheral area (**B**). There is a rapid decline in vascularity adjacent to and within the necrotic core of the larger prostate tumors (**C**).

Table III. Image analysis of blood vessels

	Blood vessels (vessels/HPF)	Diameter (mean, μm)	Blood vessel (% area/HPF)	Roundness (round = 1.0)
NSPC sites* (n = 54)	3.8 ± 1.7[a]	38.4 ± 23.7[a]	0.30 ± 0.33[a]	2.2 ± 0.9[a]
Hyperplasia (n = 16)	11.8 ± 5.5[b]	28.5 ± 8.5[a,b]	0.56 ± 0.34[a]	2.7 ± 0.5[a,b]
Atypical hyperplasia (n = 15)	15.0 ± 6.8[b,c,d]	25.5 ± 7.9[b]	0.47 ± 0.31[b]	3.1 ± 1.0[b]
Well-differentiated adenocarcinoma (n = 11)	15.4 ± 4.4[b,c]	33.8 ± 9.0[a,b]	1.00 ± 0.56[a,b]	2.6 ± 0.7[a,b]
Moderately-differentiated adenocarcinoma (n = 6)	23.6 ± 9.9[d]	37.1 ± 33.3[a,b]	0.82 ± 0.80[a,b]	3.0 ± 0.4[b]
Poorly-differentiated adenocarcinoma (n = 20)	45.0 ± 20.3[e]	35.1 ± 8.6[a,b]	3.68 ± 1.93[c]	2.5 ± 0.8[a,b]

The data represent the mean ± SD. Mean with different superscript indicates $P < 0.05$ by one-way ANOVA and Fisher's protected least significant difference. *NSPC, no significantly pathological change.

we have reported that diet restriction reduces tumor growth primarily through an increase in apoptosis rather than reduced proliferation (21).

Our results and the published literature regarding apoptosis during prostate carcinogenesis may suggest a paradox to some readers. If resistance to apoptotic signals is a fundamental characteristic of cancer cells (10), one may hypothesize that the proportion of apoptotic cells (apoptotic index) should decrease as malignancy progresses, which is the opposite of the observations. We certainly agree that apoptotic resistance is a key characteristic of prostate cancer cells, in part due to the accumulated defects in the intracellular pathways that constitutively activate linked proliferative and survival signals. However, resistance to apoptosis is not absolute, but a relative resistance. As tumors progress we believe that the tumor microenvironment becomes more stressful for cellular survival,

especially in terms of poor oxygenation, rising interstitial pressure and accumulated metabolic waste. These and other factors contribute to the gradual rise in apoptosis observed as tumors expand in size due to the accelerating proliferative rate associated with more aggressive cancers.

Tumor growth beyond a few millimeters in size is critically dependent upon angiogenesis in order to provide essential nutrients, oxygen and the removal of metabolic waste from the tumor (15). Evidence is emerging that tumor angiogenesis is also a key component of prostate cancer progression. The optimal methods to quantify biomarkers of angiogenesis in tissues such as vascular density with endothelial markers, growth factor expression such as VEGF or growth factor receptors continue to be developed. Vascular density, a measurement of the number of vascular structures in a tissue section has emerged as a biomarker that integrates the many processes involved in tumor angiogenesis. The majority of human studies (41–45) employ CD34, CD31 and factor VIII as the endothelial targets for immunohistochemical analysis. Quantification of stained structures within the 'hot spot' is typically based upon the manual counting of vessels in a high-powered field by investigators. Several studies report that intratumoral MVD in human prostate carcinoma is higher than normal prostate tissue (41–43). Furthermore, vascularity is associated with more advanced prostate tumor Gleason grade or stage (46–49). Prostate tumor MVD may prove to be an independent prognostic factor for advanced pathological stage or metastasis (44,45,48–54) or cancer-specific survival in patients with grade II tumors (WHO) (55). It is proposed that the combination of Gleason score and MVD enhances the ability to predict preoperatively extraprostatic extension of cancer (56). However, it is important to note that some studies showed inconsistent results for the association of MVD with pathologic stage, tumor grade and clinical outcome in prostate cancer (57,58). Our studies with the MNU model also show a very strong association between MVD and tumor grade and stage. Our observations in the MNU model of prostate carcinogenesis are consistent with the hypothesis that angiogenesis is an essential component in the development of more aggressive prostate tumors; thus, this system may be useful in elucidating mechanisms responsible for the angiogenic switch. Furthermore, the MNU model may allow investigators to evaluate dietary or chemopreventive agents that specifically target growth factors and inhibitors involved in angiogenesis. In other models of prostate carcinogenesis, our laboratory has shown that dietary interventions such as energy restriction and the consumption of soy products can reduce tumor growth in parallel with a reduction in tumor vascularity (21,59) suggesting that dietary components may directly or indirectly influence the angiogenic phenotype.

The human prostate is heterogeneous in histologic features and biomarker expression, in part due to the different anatomical components of the normal gland (23,33). Furthermore, human prostate cancer is often multifocal and immunohistochemical, molecular and genetic biomarkers may vary among different islands of cancer within the prostate gland (24,29,32,33,60,61). There are few studies in the humans or rodent prostate cancer evaluating the variation in PCNA labeling, apoptotic index and vascular density within the tumor microenvironment. In one human study, the periphery of the cancer exhibits higher PCNA counts (11.76 ± 0.74%) than the central areas (5.97 ± 0.32%) (21). As MNU prostate tumors become invasive and expand in size we see a predictable spatial relationship for biomarkers within the tumor. The outmost 500 mm of the cancer, especially along the serosal surface appears as a rim of malignant cells that exhibit less proliferation, a modest network of blood vessels and low apoptosis. In comparison, the area we call the intermediate zone extending from 500 mm to several millimetres towards the central necrotic core often contains a dense array of poorly formed vascular channels of variable size and shape. It is this area of the tumor that also exhibits the highest rate of PCNA labeling, but lower apoptosis in this region. These vessels are often irregular, tortuous and sinusoidal with ill-formed endothelial lining or basement membranes, as observed in human prostate cancer. Most of the poorly differentiated and larger tumors exhibit a central core containing sheets or patches of cells that are in various stages of necrosis with low rates of PCNA labeling, the highest rates of ApoTag staining, and few small and compressed vessels detected by immunohistochemistry. The necrotic cores result from poor perfusion and removal of metabolic waste in conjunction with the rising interstitial pressure and hypoxia (14,63). It is possible that the reduced apoptosis in the intermediate zone is related to the greater vascularity allowing more efficient nutrient and oxygen availability and a lower rate of apoptosis. In addition, greater vascularity may allow more efficient infiltration of phagocytes such as macrophages and other inflammatory cells that dispose and clear apoptotic debris. Thus, the more efficient vasculature in the intermediate zone may enhance survival of cells as well as promote a more rapid clearance of apoptotic cells leading to the lower apoptotic index. We conclude that like human cancer, predictable spatial variation in biomarker expression is noted within larger tumors in the MNU model and should be taken into consideration in the evaluation of biomarkers following interventions.

These studies provide valuable histopathologic and biomarker data regarding the MNU androgen-induced model of prostate carcinogenesis that may be useful in future studies designed for the pre-clinical evaluation of dietary interventions and chemopreventive agents. We have independently confirmed the observations of others (5–7), that this model demonstrates a gradient of histopathologic features consistent with human prostate cancer progression. Proliferation index, apoptotic index and MVD are easily and objectively quantified by immunohistochemical staining and digital computerized image analysis in order to provide quantitative data regarding histologic outcome. Newer methodologic and statistical approaches to computerized image analysis of histopathologic biomarkers include grid-point techniques that will further reduce the bias associated with selecting areas for quantification and improve the precision and predictive value of the analysis. Prostate carcinogenesis in this model is associated with a profound dysregulation of proliferation as indicated by the dramatic increase in the proportion of cells undergoing division (PCNA labeling) as the prostate lesions become more aggressive. In addition, this model exhibits a progressive increase in tumor vascularity as carcinogenesis progresses. Apoptosis is also related positively to the progression of cancer in this model, but is best understood in the context of intratumoral geography and its inverse relationship to intratumoral vascularity. The changes in proliferation, apoptosis and angiogenesis exhibit a

predictable pattern as prostate cancer progresses in this model and thus provides an excellent opportunity to examine molecular mechanisms linking these critical processes. We conclude that this model is an excellent system for the evaluation of dietary and chemopreventive agents that may reduce the risk of prostate cancer or improve its treatment.

Acknowledgements

The authors thank Kimberly Carter, Dahlys Hoot and Valerie DeGroff for technical assistance. This study was supported by the Public Health Service, National Institutes of Health, National Cancer Institute, RO1-CA72482 to S.K.C, NRI-U.S. Department of Agriculture program agreement #95-37200 to J.W.E., and the Comprehensive Cancer Center, The Ohio State University Grant P30-CA16058, National Cancer Institute and the Prostate Cancer Fund of the Arthur G.James Cancer Hospital.

References

1. Xie,W., Wong,Y.C. and Tsao,S.W. (2000) Correlation of increased apoptosis and proliferation with development of prostatic intraepithelial neoplasia (PIN) in ventral prostate of the Noble rat. *Prostate*, **44**, 31–39.
2. Shiina,H., Igawa,M., Shigeno,K. *et al.* (1997) Immunohistochemical analysis of estramustine binding protein with particular reference to proliferative activity in human prostatic carcinoma. *Prostate*, **32**, 49–58.
3. Martin,J.J., Martin,R., Codesal,J., Fraile,B., Paniagua,R. and Santamaria,L. (2001) Cadmium chloride-induced dysplastic changes in the ventral rat prostate: an immunohistochemical and quantitative study. *Prostate*, **46**, 11–20.
4. Bosland,M.C. (1992) Animal models for the study of prostate carcinogenesis. *J. Cell. Biochem. Suppl.*, **16H**, 89–98.
5. McCormick,D.L., Rao,K.V., Dooley,L., Steele,V.E., Lubet,R.A., Kelloff,G.J. and Bosland,M.C. (1998) Influence of *N*-methyl-*N*-nitrosourea, testosterone and *N*-(4-hydroxyphenyl)-all-*trans*-retinamide on prostate cancer induction in Wistar-Unilever rats. *Cancer Res.*, **58**, 3282–3288.
6. Bosland,M.C. and Prinsen,M.K. (1990) Induction of dorsolateral prostate adenocarcinomas and other accessory sex gland lesions in male Wistar rats by a single administration of *N*-methyl-*N*-nitrososourea, 7,12-dimethylbenz(a)anthracene and 3,2′-dimethyl-4-aminobiophenyl after sequential treatment with cyproterone acetate and testosterone propionate. *Cancer Res.*, **50**, 691–699.
7. Bosland,M.C., Prinsen,M.K. and Kroes,R. (1983) Adenocarcinomas of the prostate induced by *N*-nitroso-*N*-methylurea in rats pretreated with cyproterone acetate and testosterone. *Cancer Lett.*, **18**, 69–78.
8. McCormick,D.L. and Rao,K.V. (1999) Chemoprevention of hormone-dependent prostate cancer in the Wistar-Unilever rat. *Euro. Urol.*, **35**, 464–467.
9. Kelloff,G.J., Sigman,C.C., Hawk,E.T., Johnson,K.M., Crowell,J.A. and Guyton,K.Z. (2001) *Surrogate End-point Biomarkers in Chemopreventive Drug Development*. IARC Scientific Publications No. 154, IARC, Lyon, pp. 13–26.
10. Hanahan,D. and Weinberg,R.A. (2000) The hallmarks of cancer. *Cell*, **100**, 57–70.
11. Isaacs,J.T. (2000) Apoptosis: translating theory to therapy for prostate cancer. [letter; comment]. *J. Natl Cancer Inst.*, **92**, 1367–1369.
12. Vukanovic,J. and Isaacs,J.T. (1995) Human prostatic cancer cells are sensitive to programmed (apoptotic) death induced by the antiangiogenic agent linomide. *Cancer Res.*, **55**, 3517–3520.
13. Folkman,J. (1995) Angiogenesis in cancer, vascular, rheumatoid and other disease. *Nature Med.*, **1**, 27–31.
14. Folkman,J. (1971) Tumor angiogenesis: therapeutic implications. *N. Engl. J. Med.*, **285**, 1182–1186.
15. Folkman,J. (1992) The role of angiogenesis in tumor growth. *Cancer Biol.*, **3**, 65–71.
16. Boileau,T.W.-M., Clinton,S.K., Liao,Z. and Erdman,J.W. Jr (2001) Tomato phytochemicals and diet restriction increase survival of rats with *N*-methyl-*N*-nitrosourea (MNU)-testosterone-induced prostate cancer. *FASEB J.*, **15**, A618.
17. Reeves,P.G. (1993) AIN-93 purified diets for laboratory rodents: final report of the American Institute of Nutrition ad hoc writing committee on the reformulation of the AIN-76A rodent diet. *J. Nutr.*, **123**, 1939–1951.
18. Kelman,Z. (1997) PCNA: structure, functions and interactions. *Oncogene*, **14**, 629–640
19. Gavrieli,Y., Sherman,Y. and Ben-Sasson,S.A. (1992) Identification of programmed cell death *in situ* via specific labeling of nuclear DNA fragmentation. *J. Cell. Biol.*, **119**, 493–501.
20. Kawamura,K., Kobayashi,Y., Tanaka,T., Ikeda,R., Fujikawa-Yamamoto,K. and Suzuki,K. (2000) Intranuclear localization of proliferating cell nuclear antigen during the cell cycle in renal cell carcinoma. *Anal. Quant. Cyto. Hist.*, **22**, 107–113.
21. Mukherjee,P., Sotnikov,A.V., Mangian,H.J., Zhou,J.-R., Visek,W.J. and Clinton,S.K. (1999) Energy intake and prostate tumor growth, angiogenesis and vascular endothelial growth factor expression. *J. Natl Cancer Inst.*, **91**, 512–523.
22. Montironi,R., Galluzzi,C.M., Diamanti,L., Giannulis,I., Scarpelli,M. and De Nictolis,M. (1993) Proliferating cell nuclear antigen (PCNA) in prostatic invasive adenocarcinoma. Is the proliferation state in the marginal zone of the tumour higher than in the central part? *Anticancer Res.*, **13**, 129–132.
23. Montironi,R., Galluzzi,C.M., Diamanti,L., Giannulis,I., Pisani,E. and Scarpelli,M. (1993) Prostatic intra-epithelial neoplasia: expression and location of proliferating cell nuclear antigen in epithelial, endothelial and stromal nuclei. *Virch. Archiv. A Pathol. Anat. Histopath.*, **422**, 185–192.
24. Kallakury,B.V., Sheehan,C.E., Rhee,S.J., Fisher,H.A., Kaufman,R.P. Jr, Rifkin,M.D. and Ross,J.S. (1999) The prognostic significance of proliferation-associated nucleolar protein p120 expression in prostate adenocarcinoma: a comparison with cyclins A and B1, Ki-67, proliferating cell nuclear antigen and p34cdc2. *Cancer*, **85**, 1569–1576.
25. Burger,P., Shibata,T. and Kleihues,P. (1986) The use of the monoclonal antibody Ki-67 in the identification of proliferating cells: application to surgical neuropathology. *Am. J. Surg. Pathol.*, **10**, 611–617.
26. Sadi,M.V. and Barrack,E.R. (1991) Determination of growth fraction in advanced prostate cancer by Ki-67 immunostaining and its relationship to the time to tumor progression after hormonal therapy. *Cancer*, **67**, 3065–3071.
27. Cheng,L., Pisansky,T.M., Sebo,T.J., Leibovich,B.C., Ramnani,D.M., Weaver,A.L., Scherer,B.G., Blute,M.L., Zincke,H. and Bostwick,D.G. (1999) Cell proliferation in prostate cancer patients with lymph node metastasis: a marker for progression. *Clin. Cancer Res.*, **5**, 2820–2823.
28. Bostwick,D.G., Burke,H.B., Wheeler,T.M., Chung,L.W., Bookstein,R., Pretlow,T.G., Nagle,R.B., Montironi,R., Lieber,M.M. and Veltri,R.W. (1994) The most promising surrogate endpoint biomarkers for screening candidate chemopreventive compounds for prostatic adenocarcinoma in short-term phase II clinical trials. *J. Cell. Biochem. Suppl.*, **19**, 283–289.
29. Vacherot,F., Azzouz,M., Gil-Diez-De-Medina,S., Colombel,M., De La Taille,A., Lefrere Belda,M.A., Abbou,C.C., Raynaud,J.P. and Chopin,D.K. (2000) Induction of apoptosis and inhibition of cell proliferation by the lipido-sterolic extract of Serenoa repens (LSESr) Permixon in benign prostatic hyperplasia. *Prostate*, **45**, 259–266.
30. Vesalainen,S., Lipponen,P., Talja,M. and Syrjanen,K. (1995) Mitotic activity and prognosis in prostatic adenocarcinoma. *Prostate*, **26**, 80–86.
31. Giannulis,I., Montironi,R., Galluzzi,C.M., de Nictolis,M. and Diamanti,L. (1993) Frequency and location of mitoses in prostatic intraepithelial neoplasia (PIN). *Anticancer Res.*, **13**, 2447–2451.
32. Colombel,M., Vacherot,F., Diez,S.G., Fontaine,E., Buttyan,R. and Chopin,D. (1998) Zonal variation of apoptosis and proliferation in the normal prostate and in benign prostatic hyperplasia. *Br. J. Urol.*, **82**, 380–385.
33. Montironi,R., Magi Galluzzi,C.M., Marina,S. and Diamanti,L. (1994) Quantitative characterization of the frequency and location of cell proliferation and death in prostate pathology. *J. Cell. Biochem. Suppl.*, **19**, 238–245.
34. Wheeler,T.M., Rogers,E., Aihara,M., Scardino,P.T. and Thompson,T.C. (1994) Apoptotic index as a biomarker in prostatic intraepithelial neoplasia (PIN) and prostate cancer. *J. Cell. Biochem. Suppl.*, **19**, 202–207.
35. Stapleton,A.M., Zbell,P., Kattan,M.W., Yang,G., Wheeler,T.M., Scardino,P.T. and Thompson,T.C. (1998) Assessment of the biologic markers p53, Ki-67 and apoptotic index as predictive indicators of prostate carcinoma recurrence after surgery. *Cancer*, **82**, 168–175.
36. Aihara,M., Truong,L.D., Dunn,J.K., Wheeler,T.M., Scardino,P.T. and Thompson,T.C. (1994) Frequency of apoptotic bodies positively correlates with Gleason grade in prostate cancer. *Hum. Pathol.*, **25**, 797–801.
37. Glassman,D.T., Chon,J.K., Borkowski,A., Jacobs,S.C. and Kyprianou,N. (2001) Combined effect of terazosin and finasteride on apoptosis, cell proliferation and transforming growth factor-beta expression in benign prostatic hyperplasia, *Prostate*, **46**, 45–51.
38. Kyprianou,N., English,H.F. and Isaacs,J.T. (1990) Programmed cell death during regression of PC-82 human prostate cancer following androgen ablation. *Cancer Res.*, **50**, 3748–3753.
39. Kyprianou,N. and Isaacs,J.T. (1988) Activation of programmed cell death in the rat ventral prostate after castration. *Endocrinology*, **122**, 552–562.

40. English,H.F., Kyprianou,N. and Isaacs,J.T. (1989) Relationship between DNA fragmentation and apoptosis in the programmed cell death in the rat prostate following castration. *Prostate*, **15**, 233–250.
41. Bettencourt,M.C., Bauer,J.J., Sesterhenn,I.A., Connelly,R.R. and Moul,J.W. (1998) CD34 immunohistochemical assessment of angiogenesis as a prognostic marker for prostate cancer recurrence after radical prostatectomy. *J. Urol.*, **160**, 459–465.
42. Brawer,M.K., Bigler,S.A. and Deering,R.E. (1992) Quantitative morphometric analysis of the microcirculation in prostate carcinoma. *J. Cell. Biochem. Suppl.*, **16H**, 62–64.
43. Bigler,S.A., Deering,R.E. and Brawer,M.K. (1993) Comparison of microscopic vascularity in benign and malignant prostate tissue. *Hum. Pathol.*, **24**, 220–226.
44. Rogatsch,H., Hittmair,A., Reissigl,A., Mikuz,G. and Feichtinger,H. (1997) Microvessel density in core biopsies of prostatic adenocarcinoma: a stage predictor? *J. Pathol.*, **182**, 205–210.
45. Matsushima,H., Goto,T., Hosaka,Y., Kitamura,T. and Kawabe,K. (1999) Correlation between proliferation, apoptosis and angiogenesis in prostate carcinoma and their relation to androgen ablation. *Cancer*, **85**, 1822–1827.
46. Vartanian,R.K. and Weidner,N. (1995) Endothelial cell proliferation in prostatic carcinoma and prostatic hyperplasia: correlation with Gleason's score, microvessel density and epithelial cell proliferation. *Lab. Invest.*, **73**, 844–850.
47. Brawer,M.K., Deering,R.E., Brown,M., Preston,S.D. and Bigler,S.A. (1994) Predictors of pathologic stage in prostatic carcinoma. The role of neovascularity. *Cancer*, **73**, 678–687.
48. Silberman,M.A., Partin,A.W., Veltri,R.W. and Epstein,J.I. (1997) Tumor angiogenesis correlates with progression after radical prostatectomy but not with pathologic stage in Gleason sum 5 to 7 adenocarcinoma of the prostate. *Cancer*, **79**, 772–779.
49. Mydlo,J.H., Kral,J.G., Volpe,M., Axotis,C., Macchia,R.J. and Pertschuk,L.P. (1998) An analysis of microvessel density androgen receptor, p53 and HER-2/neu expression and Gleason score in prostate cancer. preliminary results and therapeutic implications. *Eur. Urol.*, **34**, 426–432.
50. Wakui,S., Furusato,M., Itoh,T., Sasaki,H., Akiyama,A., Kinoshita,I., Asano,K., Tokuda,T., Aizawa,S. and Ushigome,S. (1992) Tumour angiogenesis in prostatic carcinoma with and without bone marrow metastasis: a morphometric study. *J. Pathol.*, **168**, 257–262.
51. Fregene,T.A., Khanuja,P.S., Noto,A.C., Gehani,S.K., Van Egmont,E.M., Luz,D.A. and Pienta,K.J. (1993) Tumor associated angiogenesis in prostate cancer. *Anticancer Res.*, **13**, 2377–2382.
52. Weidner,N., Carroll,P.R., Flax,J., Blumenfeld,W. and Folkman,J. (1993) Tumor angiogenesis correlates with metastasis in invasive prostate carcinoma. *Am. J. Pathol.*, **143**, 401–409.
53. Vesalainen,S.L., Lipponen,P.K., Talja,M.T., Alhava,E.M. and Syrjanen,K.J. (1994) Proliferating cell nuclear antigen and p53 expression as prognostic factors in T1-2M0 prostatic adenocarcinoma. *Int. J. Cancer*, **58**, 303–308.
54. Barth,P.J., Weingartner,K., Kohler,H.H. and Bittinger,A. (1996) Assessment of the vascularization in prostatic carcinoma: a morphometric investigation. *Hum. Pathol.*, **27**, 1306–1310.
55. Lissbrant,I.F., Stattin,P., Damber,J.E. and Bergh,A. (1997) Vascular density is a predictor of cancer-specific survival in prostatic carcinoma. *Prostate*, **33**, 38–45.
56. Bostwick,D., Wheeler,T., Miles,B., Scardino,P., Humphrey,P., Hudson,M.L.A. and Mahran,H. (1996) Optimized microvessel density analysis improves prediction of cancer stage from prostate needle biopsies. *J. Urol.*, **155**, 554A.
57. Gettman,M.T., Bergstralh,E.J., Blute,M., Zincke,H. and Bostwick,D.G. (1998) Prediction of patient outcome in pathologic stage T2 adenocarcinoma of the prostate: lack of significance for microvessel density analysis. *Urology*, **51**, 79–85.
58. Rubin,M.A., Buyyounouski,M., Bagiella,E., Sharir,S., Neugut,A., Benson,M., de la Taille,A., Katz,A.E., Olsson,C.A. and Ennis,R.D. (1999) Microvessel density in prostate cancer: lack of correlation with tumor grade, pathologic stage and clinical outcome. *Urology*, **53**, 542–547.
59. Zhou,J.-R., Gugger,E.T., Tanaka,T., Guo,Y., Blackburn,G.L. and Clinton,S.K. (1999) Soybean phytochemicals inhibit the growth of transplantable human prostate carcinoma and tumor angiogenesis in mice. *J. Nutr.*, **129**, 1628–1635.
60. Fukagai,T., Namiki,T., Namiki,H., Carlile,R.G., Shimada,M. and Yoshida,H. (2001) Discrepancies between Gleason scores of needle biopsy and radical prostatectomy specimens. *Pathol. Int.*, **51**, 364–370.
61. Nwosu,V., Carpten,J., Trent,J. and Sheridan,R. (2001) Heterogeneity of genetic alterations in prostate cancer: evidence of the complex nature of the disease. *Hum. Mol. Genet.*, **10**, 2313–8.
62. Brown,J. and Giaccia,A. (1998) The unique physiology of solid tumors: opportunities (and problems) for cancer therapy. *Cancer Res.*, **58**, 1408–1416.
63. Folkman,J. (1995) Clinical applications of research on angiogenesis. *N. Engl. J. Med.*, **333**, 1757–1763

Received April 8, 2002; revised and accepted May 30, 2002